Sinop University
Journal of Positive Science International
e-ISSN: 3108-3862

Journal of Positive Science International, 1(2), 86-102
Research Article
Year: 2025

A Comprehensive Analysis of the Internal Ballistic Effects of Riffled Barrels

Ahmet Furkan ÖZBİLGE[1*], Mustafa BOZDEMİR[2]

[1] *Department of Defense Technologies, Institute of Science, Kırıkkale University, Kırıkkale, Türkiye*

[2] *Department of Mechanical and Metal Technologies, Kırıkkale Vocational High School, Kırıkkale University, Kırıkkale, Türkiye*

Article Info

Research article
Received: *11.08.2025*
Revision: *09.12.2025*
Accepted: *12.12.2025*
Published: *30.12.2025*
***Corresponding Author*:** *Ahmet Furkan ÖZBİLGE*
ozbilge95@gmail.com
0009-0008-4464-4146

Keywords

Internal Ballistics
Rifled Barrel Design
Ammunition
Ballistic Analysis
ANSYS
FEA

Abstract

This study examines how rifled barrel geometries influence internal ballistic behavior under high-pressure conditions through explicit dynamic simulations in ANSYS. Barrel length, rifling angle and configuration, propellant mass, and projectile nose curvature radius were varied individually across seven models to isolate their effects. Results show that longer barrels increase muzzle velocity but also deformation; larger rifling angles improve rotational stability while reducing linear acceleration due to frictional losses; changes in nose curvature radius significantly alter both deformation and velocity; and increased propellant mass enhances acceleration but may reduce energy efficiency when mismatched with barrel geometry. Overall, the study offers essential guidance for understanding and optimizing rifled barrel parameters in internal ballistic applications.

Yiv-setli Namluların İç Balistiğe Etkisinin Kapsamlı İncelenmesi

Makale Bilgisi

Araştırma makalesi
Başvuru: *11.08.2025*
Düzeltme: *09.12.2025*
Kabul: *12.12.2025*
Yayın*: 30.12.2025*
***Sorumlu Yazar*:** *Ahmet Furkan ÖZBİLGE*
ozbilge95@gmail.com
0009-0008-4464-4146

Anahtar Kelimeler

İç Balistik
Yiv-setli Namlu Tasarımı
Mühimmat
Balistik Analiz
ANSYS
Sonlu Elemanlar Analizi (FEA)

Özet

Bu çalışma, yivli namlu geometrilerinin yüksek basınç koşullarındaki iç balistik davranış üzerindeki etkilerini ANSYS'te yürütülen explicit dinamik simülasyonlar aracılığıyla incelemektedir. Namlu boyu, yiv açısı ve yiv yapısı, barut kütlesi ve mermi burun yarıçapı olmak üzere dört temel parametre, etkilerini ayrı ayrı değerlendirmek amacıyla yedi model üzerinde tek değişkenli yaklaşım ile analiz edilmiştir. Sonuçlar, uzun namluların çıkış hızını artırırken deformasyonu da yükselttiğini; geniş yiv açılarının dönme stabilitesini iyileştirse de sürtünmeden kaynaklı enerji kayıpları nedeniyle doğrusal hızını azalttığını; burun geometrisindeki değişimlerin hem deformasyon hem de hız üzerinde belirgin etkiler oluşturduğunu; barut kütlesinin artışının ise uygun olmayan geometrilerde enerji verimliliğini düşürebildiğini göstermektedir. Genel olarak çalışma, iç balistik performansın optimize edilmesi için yivli namlu parametrelerinin anlaşılmasına ve doğru şekilde seçilmesine yönelik önemli bir bilimsel referans sunmaktadır.

To cite this article:
Özbilge, F. A., & Bozdemir, M. (2025). A Comprehensive Analysis of the Internal Ballistic Effects of Riffled Barrels, Positive Science International, 1(2), 86-102

1. Introduction

Internal ballistics, a subfield of ballistics, focuses on the physical processes that occur within a firearm barrel between the initiation of the propellant charge and the projectile's exit. This field plays a vital role in understanding the internal pressure dynamics, projectile acceleration, and structural stresses that occur during firing. Among the most influential design elements in this phase are rifled barrel characteristics, ammunition volume, and barrel length—all of which significantly affect the behavior of the projectile and the mechanical response of the firearm components.

The optimization of internal ballistic performance has become essential for enhancing the accuracy, efficiency, and reliability of modern weapon systems. Innovations in computational modeling have enabled detailed exploration of dynamic processes that were previously difficult to measure experimentally. In this context, finite element analysis (FEA) methods, particularly using simulation platforms such as ANSYS, have provided a robust analytical framework for modeling internal ballistic interactions and evaluating material behavior under high-pressure conditions.

This study investigates how variations in rifling geometry, barrel length, and internal volume influence key parameters such as projectile exit velocity, deformation, and contact pressure distribution. By simulating different barrel configurations, the research aims to provide a comparative assessment of ballistic outcomes and uncover design implications relevant to defense engineering and firearm development.

2. Materials And Method

In this study, the internal ballistic performance of rifled barrels was investigated through finite element simulations using ANSYS Workbench. Various barrel models were designed with distinct geometrical parameters such as barrel length, rifling geometry, and internal volume. The objective was to assess how these variables influence critical internal ballistic outcomes, including projectile velocity, structural deformation, and internal stress distribution.

The simulation process was based on a transient structural analysis approach. High-pressure loading, resulting from the ignition of the propellant, was applied to the base of the projectile. Material properties for both the barrel and projectile were defined using experimentally validated mechanical data, and nonlinear material behavior under dynamic conditions was considered.

Each model incorporated rifling features with consistent twist angles and calibers to isolate the effect of barrel length and internal volume. Mesh optimization was performed to balance computational efficiency and result accuracy. Time-step sensitivity analysis was also conducted to ensure the stability and convergence of the simulations.

Post-processing operations were carried out to extract projectile velocity profiles, deformation patterns, and pressure contours. These results were then comparatively evaluated to reveal design implications related to barrel efficiency and structural integrity.

In modern armament design, the internal ballistic phase—covering the projectile's movement within the barrel—is critically influenced by rifling geometry, barrel dimensions, and propellant characteristics (1,2). The objective of this study is to investigate how different rifled barrel configurations affect projectile deformation and muzzle velocity by means of computational simulations. Finite Element Analysis (FEA)-based simulations offer an effective approach for analyzing structural and dynamic interactions within the high-strain and high-pressure regime characteristic of internal ballistics (3,4).

2.1. Barrel and Projectile Design

A series of barrel geometries were developed, varying in terms of:

- Barrel length (300 mm and 500 mm),
- Rifling configurations (groove count × twist rate),
- Projectile Nose Curvature Radius ,
- Propellant layer thickness (3 mm and 5 mm).

All models were designed in accordance with axisymmetric and solid mechanical principles. To isolate variables effectively, each barrel configuration differed by only one parameter at a time (e.g., rifling geometry or curvature radius), enabling a controlled comparative analysis (1,5).

2.2. Simulation Platform and Setup

Finite element simulations were performed using ANSYS Workbench with *Explicit Dynamics* solvers, which are suitable for transient events involving high strain rates and complex contact interactions (6). Structural contact definitions were assigned between barrel and projectile surfaces with frictional behavior, and nonlinear material behavior under large deformations was included (7).

Time integration was conducted via an explicit Lagrangian formulation, ensuring accurate resolution of transient impact behavior.

Contact algorithms were refined using penalty-based contact models for computational stability.

The projectile was subjected to pressure loading at the base surface, representing ignition-induced propellant gas pressure.

2.3. Material Modeling

Materials for the barrel and projectile were assigned based on experimentally validated mechanical properties, including:

- Density (ρ),
- Elastic modulus (E),
- Yield strength (σ_y),
- Strain-rate sensitive plasticity models.

These parameters were defined based on high strain-rate studies of steel and alloyed copper typically used in small and medium caliber munitions (8,9).

2.4. Mesh and Time-Step Optimization

Mesh convergence and time-step sensitivity analyses were performed:

Mesh Optimization: Fine mesh resolution near rifling grooves and projectile contact surfaces was applied using body sizing and adaptive refinement techniques.

Time-Step Control: Minimum time-step criteria were governed by Courant-Friedrichs-Lewy (CFL) conditions to prevent solution divergence (6,10).

2.5. Post-Processing and Data Evaluation

Simulation outputs included:

- **Projectile Muzzle Velocity**: Extracted from the final time step using nodal velocity data,
- **Maximum Total Deformation**: Obtained from element strain results,
- **Pressure Contours**: Visualized for qualitative flow behavior along barrel interior.

These results were evaluated comparatively to identify performance trends across different rifling and barrel geometries. Special attention was given to cases where deformation compromises projectile stability or excessive stress exceeds material limits (1,7,9).

The numerical results suggest that rifling density and nose curvature radius exert competing influences on deformation and velocity. Denser rifling increases rotational torque at the cost of greater structural deformation, while more gradual projectile nose geometry improves gas flow uniformity and pressure utilization. These findings provide key design insights for optimizing barrel configurations based on specific mission requirements and performance thresholds (2,4,8).

3. Results & Discussion

In this study, seven different barrel configurations were analysed. While the barrels varied in terms of geometric dimensions, rifling angles, propellant mass, projectile nose geometry, and the helix angle of the rifling relative to the horizontal axis, several parameters were kept constant across all models. These included the bore diameter, barrel wall thickness, selected barrel steel properties, and the baseline propellant characteristics. To ensure a more accurate and numerically stable simulation, the rear section of each barrel was fully constrained and modelled as a closed boundary.

Additionally, the geometric thickness of the propellant layer was kept identical for the first six barrels, whereas in Barrel-7 this thickness—and consequently the propellant mass—was deliberately increased. Because a predefined propellant material was not available in ANSYS, an explosive material model with properties closest to small-arms propellant was selected, and the relevant input parameters were adjusted accordingly. These values are presented in Table 1.

Table 1. Propellant Properties

Parameter	Value	Unit
Detonation Velocity	6930	m/s
Specific Energy (Energy Per Unit Mass)	1.68×10^6	J/kg
Explosion Pressure	2.1×10^{10}	Pa

In the simulations, AISI 4140 (DIN 42CrMo4, 1.7225) chromium–molybdenum alloy steel could not be selected directly from the material library. Therefore, a steel grade with properties closest to AISI 4140 was assigned, and its material parameters were adjusted to match the mechanical behavior of AISI 4140 as closely as possible. The final material properties used in the analysis are presented in Table 2.

Table 2. Barrel Steel Properties

Modules Used	Values
Young's Modulus (E)	2.00×10^{11} Pa (200 GPa)
Poisson's Ratio (ν)	0.3
Bulk Modulus (K)	1.6667×10^{11} Pa (166.67 GPa)
Shear Modulus (G)	7.6923×10^{10} Pa (76.923 GPa)
Isotropic Secant Coefficient of Thermal Expansion (α)	1.2×10^{-5} 1/°C (12×10^{-6} /°C)
Compressive Yield Strength	2.5×10^{8} Pa (250 MPa)
Tensile Ultimate Strength	4.6×10^{8} Pa (460 MPa)
Tensile Yield Strength	2.5×10^{8} Pa (250 MPa)

An alloyed copper material was assigned to the cartridge case, and its corresponding material properties are provided in Table 3.

Table 3. Projectile material Properties

Modules Used	Values
Young's Modulus	1.1×10^{11} Pa
Poisson's Ratio	0.34
Bulk Modulus	1.1458×10^{11} Pa
Shear Modulus	4.1045×10^{10} Pa
Isotropic Secant Coefficient of Thermal Expansion	1.8×10^{-5} 1/°C
Compressive Yield Strength	2.8×10^{8} Pa
Tensile Ultimate Strength	4.3×10^{8} Pa
Tensile Yield Strength	2.8×10^{8} Pa

In Table 4, the mesh parameters for each barrel configuration are presented. These parameters define the element structure and resolution used in the numerical model. By establishing consistent mesh characteristics, the simulations ensure accurate stress distribution and deformation predictions throughout the analysis.

Table 4. Mesh settings

Mesh Settings							
Barrel Code	**Element Order**	**Element Size**	**Number of Elements**	**Number of Nodes**	**Tet4**	**Hex8**	**Wedge6**
B1	Linear	0.001	484470	103434	483998	448	24
B2	Linear	0.001	487499	104038	487059	432	8
B3	Linear	0.001	298234	63855	297794	432	8
B4	Linear	0.002	38455	9726	38409	46	-
B5	Linear	0.002	61324	15369	61284	40	-
B6	Linear	0.002	38430	9720	38384	46	-
B7	Linear	0.001	484706	103657	484046	648	12

The analysis settings that define the boundary conditions are provided in Table 5. These parameters ensure that the numerical model accurately represents the physical constraints of the system. By specifying consistent loading and contact definitions, the simulations maintain stability and reliability throughout the ballistic cycle.

Table 5. Analysis settings

Analysis Settings					
Barrel Code	**X Scale Factor**	**Y Scale Factor**	**Z Scale Factor**	**Time Step Safety Factor**	**End Time**
B1	1.2	1.2	1.2	0.9	0.01
B2	1.2	1.2	1.2	0.9	0.01
B3	1.2	1.2	1.2	0.9	0.0045
B4	1.2	1.2	1.2	0.9	0.004
B5	1.2	1.2	1.2	0.9	0.005
B6	1.2	1.2	1.2	0.9	0.004
B7	1.2	1.2	1.2	0.9	0.01

The barrel wall thickness shown in Figure 1 was kept constant for all analyzed barrel configurations and was assigned a value of 3 mm.

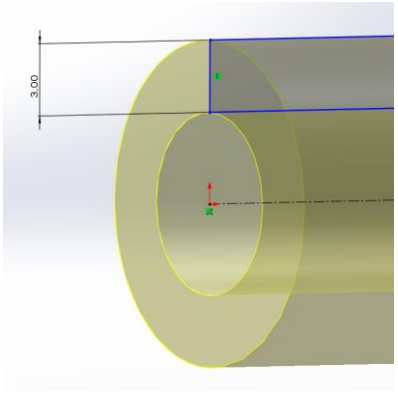

Figure 1. Barrel Wall Thickness

Figure 2 presents the number of rifling lands and grooves, as well as the rifling geometry, used in all barrel configurations analyzed in this study.

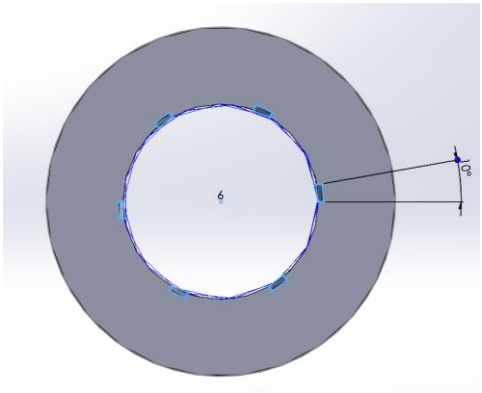

Figure 2. Number of Riflings and Rifling Geometry of the Barrels

Figure 3 provides the geometric dimensions of the rifling profiles used in all barrel configurations analyzed in this study.

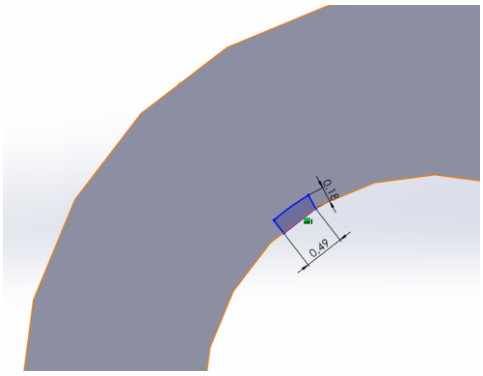

Figure 3. Rifling Geometry in the Barrels

3.1. Barrel-1 (B1) Analysis Results

In this section, the same analytical procedures were applied to all barrel configurations, and each was comprehensively evaluated. However, due to the scope limitations of the article, detailed figures and explanations are presented only for Barrel-1. The results for the remaining six barrels, obtained through the same methodology, are collectively addressed in the Comparisons section.

Table 6. Values for Barrel-1 (B1)

Barrel Parameters	Values
Diameter	7.62 mm
Barrel Length	500 mm
Rifling Configuration	100 mm'de bir 5 tur (5x100)
Helix Angle of the Rifling Relative to the Horizontal Axis	13.25°
Projectile Nose Curvature Radius	6.951 mm
Propellant Mass	0.000223 kg (223 mg)

Table 6 presents the parameter values for Barrel-1, including bore diameter, barrel length, rifling configuration, the helix angle of the rifling relative to the horizontal axis, the curvature radius of the projectile nose geometry, and the propellant mass.

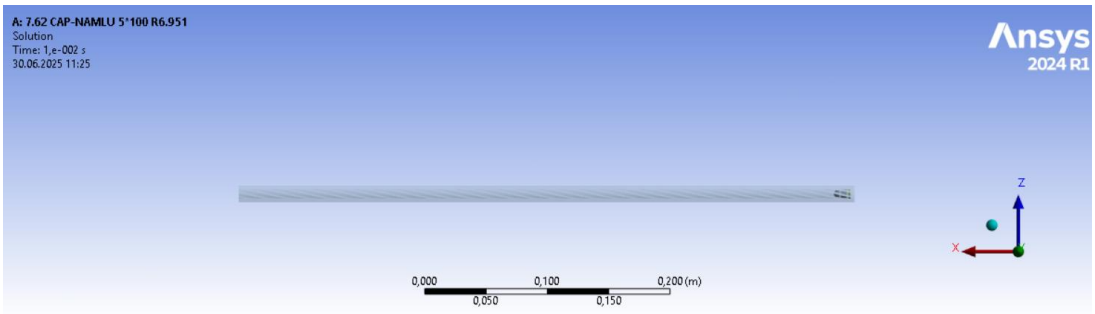

Figure 4. Representation of Barrel-1 (B1) in the ANSYS Analysis

Figure 4 shows the ANSYS interface for Barrel-1. To ensure a more accurate and stable simulation of the internal ballistic process, the rear section of the barrel was modeled as a closed boundary.

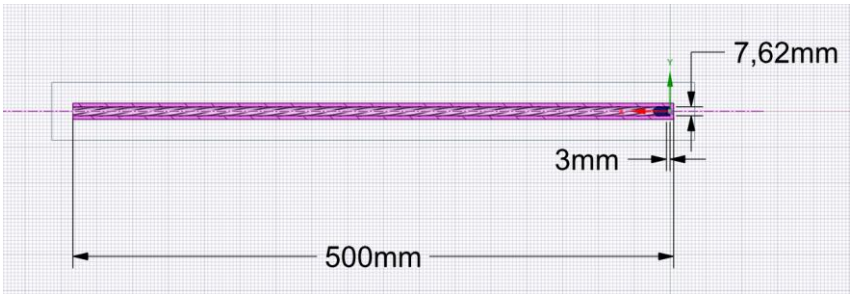

Figure 5. Geometric Dimensions of Barrel-1 (B1)

Figure 5 illustrates the geometric dimensions of Barrel-1 as displayed in the ANSYS interface. In this Figure 5, the bore diameter is specified as 7.62 mm, the barrel length as 500 mm, and the geometric thickness of the region modeled as the propellant layer within the cartridge case is given as 3 mm.

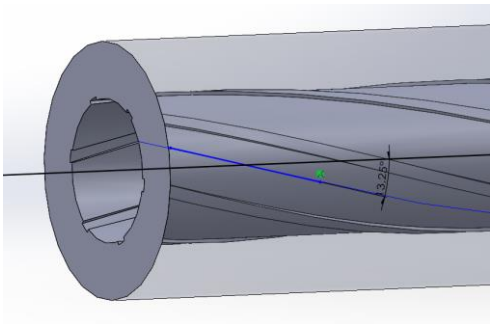

Figure 6. Helix Angle of the Rifling in Barrel-1 (B1) Relative to the Horizontal Axis

In Figure 6 the interface of the 3D solid-modeling environment shows that the helix angle of the rifling in Barrel-1 with respect to the horizontal axis is 13.25°.

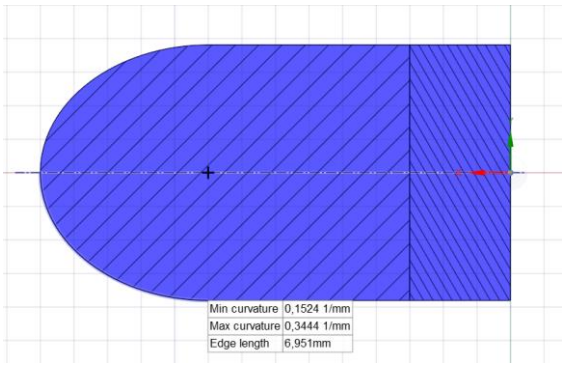

Figure 7. Curvature Radius of the Projectile Used in Barrel-1 (B1)

Figure 7 shows the curvature radius of the projectile nose geometry used in Barrel-1, as displayed in the ANSYS interface. The curvature radius of the projectile nose is given as 6.951 mm.

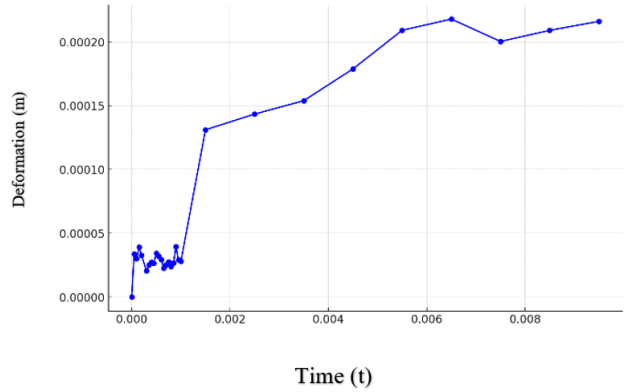

Figure 8. Barrel Deformation Graph for Barrel-1 (B1)

The Figure 8 presents the time-dependent displacement profile of Barrel-1. The maximum deformation, reaching approximately 0.22 mm, remains within the elastic regime for a high-modulus alloy steel barrel and is therefore considered mechanically acceptable under the simulated internal ballistic loading conditions. The maximum deformation, reaching approximately 0.22 mm, remains within the elastic regime for a high-modulus alloy steel barrel structure and is therefore considered mechanically acceptable under the simulated loading conditions.

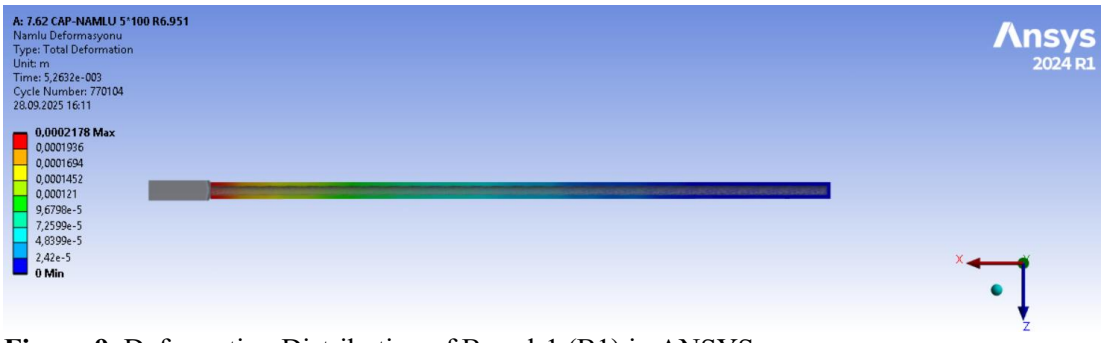

Figure 9. Deformation Distribution of Barrel-1 (B1) in ANSYS

Figure 9 presents the deformation distribution of Barrel-1 in the ANSYS environment, displayed through a contour map with color gradients representing the magnitude of deformation. The corresponding color scale illustrates the quantitative range of these displacement values.

Table 7. Barrel Deformation Values for Barrel-1 (B1)

Time [t]	Deformation [m]
0.00005	0.000034
0.00015	0.000039
0.0003	0.000021
0.00045	0.000027
0.0006	0.000029
0.00075	0.000027
0.0009	0.00004
0.001	0.000028
0.0015	0.000131
0.002	0.000137
0.0025	0.000143
0.003	0.000149
0.0035	0.000154
0.004	0.000166
0.0045	0.000179
0.005	0.000194
0.0055	0.000209
0.0065	0.000218
0.0075	0.000200
0.0095	0.000216

Table 7 presents the deformation values of Barrel-1 at selected time points from the full dataset. Although the simulation generated a larger number of deformation outputs, the table has been shortened for clarity. The maximum deformation and the corresponding time value are highlighted in red.

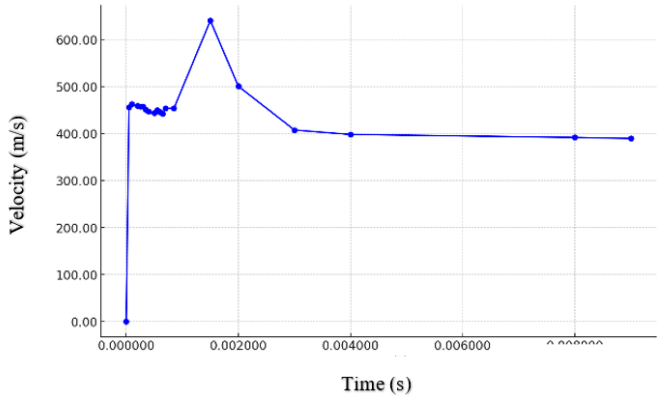

Figure 10. Total Velocity Graph of Barrel-1 (B1)

The time-dependent velocity profile presented in Figure 10 illustrates the dynamic acceleration experienced by the projectile during the internal ballistic phase. Following ignition, the projectile reaches a peak velocity of approximately 640 m/s, which also represents the muzzle velocity. After the

projectile exits the barrel, the system stabilizes around an average velocity level of approximately 400 m/s.

Table 8. Total Velocity of Barrel-1 (B1)

Time [s]	Velocity [m/s]
0.000050004	456.01
0.000100000	462.51
0.000200010	459.01
0.000250000	457.02
0.000300010	457.12
0.000350000	450.48
0.000400000	446.69
0.000500000	443.90
0.000550010	449.57
0.000600010	445.93
0.000650010	442.32
0.000700000	453.66
0.000850000	453.46
0.001500000	640.12
0.002000000	500.45
0.003000000	407.44
0.004000000	397.98
0.008000000	391.56
0.009000000	389.53

Table 8 presents the velocity values of Barrel-1 at selected time points from the full dataset. Although the simulation produced a larger number of velocity outputs, the table has been shortened for clarity. The maximum velocity (corresponding to the muzzle velocity) and the time at which it occurs are highlighted in red.

3.2. Comparisons

All comparative data are presented in Table 9.

Table 9. Comparison of Barrels

Barrel Code	Barrel Length (mm)	Rifling configuration (Turn × Twist rate)	Helix Angle of the Rifling Relative to the Horizontal Axis	Nose curvature (mm)	Propellant Mass (mg)	Maximum Barrel Deformation (mm)	Maximum Velocity (m/s)
B1	500	5 × 100	13.25°	6.951	223 mg	0.220	537.32
B2	500	2 × 250	5.65°	6.135	223 mg	0.0592	1817.5
B3	300	3 × 100	13.58°	5.5915	223 mg	0.0483	1362.5

B4	300	6 × 50	25.17°	5.902	223 mg	0.0814	1250.2
B5	500	2 × 250	5,65°	6.951	223 mg	0.29218	1817.5
B6	300	6 × 50	25,17°	5.5915	223 mg	0.28108	1227.2
B7	500	5 × 100	13.25°	6.951	371,6 mg	0.2515	582.37

Table 9 presents the parameters of seven barrels that differ from one another by a single varying variable, including barrel length, rifling angle (and the corresponding rifling configuration), projectile nose curvature, and propellant mass. For each barrel configuration, the resulting maximum deformation and maximum velocity outputs are also listed.

The comparative analysis conducted between the B1 and B5 barrel configurations clearly demonstrates the influence of rifling geometry on internal ballistic efficiency.

Table 10. Comparison of the B1 and B5 Barrel Configurations

Parameter	B1	B5
Barrel Length (mm)	500	500
Rifling Configuration	5 × 100	2 × 250
Helix Angle of the Rifling Relative to the Horizontal Axis	13.25°	5,65°
Nose Curvature Radius (mm)	6.951	6.951
Propellant Mass (mg)	223	223
Maximum Barrel Deformation(mm)	0.220	0.29218
Maximum Velocity (m/s)	537.32	1817.5

As presented in Table 10 the B1 configuration, characterized by a wider rifling angle, enhances rotational stability but limits linear velocity efficiency. (The rifling angle is directly proportional to the rifling configuration; therefore, only one variable differs between the systems.) In contrast, the B5 configuration, with its narrower rifling angle, maximizes linear acceleration capability and achieves a muzzle velocity of approximately 1817.5 m/s, demonstrating superior performance in internal ballistic energy conversion.

Although the deformation levels in both configurations remain within the elastic regime, the B5 barrel exhibits more concentrated load transfer due to its rifling geometry. Overall, the rifling design is shown to be a critical parameter that affects not only mechanical stability but also linear acceleration and energy efficiency.

Table 11. Comparison of the B2 and B5 Barrel Configurations

Parameter	B2	B5
Barrel Length (mm)	500	500
Rifling Configuration	2 × 250	2 × 250
Helix Angle of the Rifling Relative to the Horizontal Axis	5.65°	5.65°

Projectile Nose Curvature Radius (mm)	6.135	6.951
Propellant Mass (mg)	223	223
Maximum Barrel Deformation(mm)	0.0592	0.29218
Maximum Velocity (m/s)	1694.4	1817.5

The B2 and B5 configurations allow the assessment of internal ballistic performance based solely on the projectile nose geometry. Both configurations share the same barrel length, rifling angle, and propellant mass, ensuring that the nose curvature remains the only varying parameter.

As shown in Table 11, the smaller nose curvature radius in the B2 configuration (6.135 mm) results in a more localized and concentrated transfer of gas pressure, which in turn limits the maximum deformation to 0.0592 mm. In contrast, the broader nose geometry of the B5 configuration (6.951 mm) increases the contact area, leading to a higher deformation level of 0.29218 mm.

In terms of muzzle velocity, B5 surpasses B2, achieving 1817.5 m/s compared to B2's 1694.4 m/s. This difference is attributed to the more effective axial force transmission to the projectile base enabled by the larger surface area.

Overall, the projectile nose geometry directly influences both deformation behavior and velocity generation. These findings suggest that an optimal balance between minimizing deformation and maximizing velocity must be considered when selecting or designing nose shapes in ballistic systems.

Table 12. Comparison of the B3 and B6 Barrel Configurations

Parameter	**B3**	**B6**
Barrel Length (mm)	300	300
Rifling Configuration	3 × 100	6 × 50
Helix Angle of the Rifling Relative to the Horizontal Axis	13.58°	25,17°
Projectile Nose Curvature Radius (mm)	5.5915	5.5915
Propellant Mass (mg)	223	223
Maximum Barrel Deformation(mm)	0.0483	0.28108
Maximum Velocity (m/s)	1362.5	1227.2

As shown in Table 12 the B3 and B6 configurations share identical barrel length, projectile nose geometry, and propellant characteristics, isolating the effect of rifling angle on internal ballistic behavior. (The rifling angle is directly proportional to the rifling configuration; therefore, only one variable differs between the systems.) Doubling the rifling angle increases the deformation by approximately a factor of 5.8, while reducing the muzzle velocity by about 10%. This indicates that a wider rifling angle enhances the rotational moment but limits axial acceleration, leading to the accumulation of micro-straining in the barrel structure.

These results demonstrate that an engineering trade-off must be established between rotational stability and kinetic efficiency during rifling design.

Table 13. Comparison of the B4 and B6 Barrel Configurations

Parameter	B4	B6
Barrel Length (mm)	300	300
Rifling Configuration	6 × 50	6 × 50
Helix Angle of the Rifling Relative to the Horizontal Axis	25.17°	25,17°
Projectile Nose Curvature Radius (mm)	5.902	5.5915
Propellant Mass (mg)	223	223
Maximum Barrel Deformation(mm)	0.0814	0.28108
Maximum Velocity (m/s)	1250.2	1227.2

In Table 13 the B4 and B6 configurations share identical barrel length, rifling structure, and propellant mass; thus, the only varying parameter in this comparison is the projectile nose curvature. The B4 configuration, which features a broader nose geometry, produces approximately 71% less maximum deformation and achieves a muzzle velocity about 1.9% higher than that of B6. This outcome indicates that a larger curvature radius allows the gas pressure to be distributed more uniformly, thereby reducing stress concentrations at the contact surface. At the same time, it provides a more balanced acceleration profile during the aerodynamic transition.

These findings demonstrate that nose curvature is a critical design parameter that must be optimized with respect to micro-strain behavior and velocity stability.

Table 14. Comparison of the B1 and B7 Barrel Configurations

Parameter	B1	B7
Barrel Length (mm)	500	500
Rifling Configuration	5 × 100	5 × 100
Helix Angle of the Rifling Relative to the Horizontal Axis	13.25°	13.25°
Projectile Nose Curvature Radius (mm)	6.951	6.951
Propellant Mass (mg)	223	371.6
Maximum Barrel Deformation (mm)	0.220	0.2515
Maximum Velocity (m/s)	537.32	582.37

Although the B1 and B7 barrels share the same length (500 mm) and identical rifling geometry and angle, they exhibit different ballistic performance due to the variation in propellant mass.

According to Table 14 the propellant mass used in the B1 configuration is 223 mg, whereas in B7 it is increased to 371.6 mg. This increase would be expected to yield higher acceleration and muzzle velocity. However, due to the rotational resistance and frictional effects generated by the wide rifling angle, the additional energy does not fully translate into improved kinetic performance.

Although the propellant mass in B7 is increased by approximately 66%, the maximum muzzle velocity rises by only about 8.4%. This indicates low ballistic efficiency, suggesting that a significant portion of the added energy is dissipated as deformation rather than converted into kinetic energy. The

maximum deformation in B7 is 0.2515 mm, compared to 0.220 mm in B1, highlighting an increased risk of micro-straining and potential fatigue in a barrel operating near the elastic limit.

Since both barrels employ the same nose curvature (6.951 mm), no differences arise from aerodynamic exit effects. However, despite the higher propellant load in B7 supporting greater acceleration, the limiting influence of the rifling geometry prevents effective conversion of this acceleration into muzzle velocity. Consequently, B1 delivers a more balanced performance with lower energy consumption and appears to be structurally more favourable.

4. Conclusion

This study analyzes the effects of barrel geometry, rifling characteristics, projectile nose curvature, and propellant mass on internal ballistic performance using the finite element method (FEM). All simulations were conducted in the ANSYS environment. The velocity–deformation outputs obtained from various configurations were evaluated comprehensively in terms of barrel strength and energy conversion efficiency.

Barrel length directly influences muzzle velocity by increasing the duration over which gas pressure acts on the projectile. Configurations with a length of 500 mm (B1, B2, and B5) produced higher velocities compared to the 300 mm barrels (B3, B4, and B6). However, longer barrels also exhibited increased structural stress and deformation levels due to prolonged gas-pressure loading.

Rifling geometry is one of the most critical parameters governing internal ballistic performance. An increase in rifling angle enhances projectile rotational stability but simultaneously increases frictional losses and rotational resistance. In some cases, this results in greater deformation (as observed in the B3–B6 comparison), while in others, a narrower rifling angle led to increased deformation (as in the B1–B5 comparison). Overall, higher rifling angles were associated with reduced muzzle velocity.

Projectile nose curvature directly influences the distribution of gas pressure on the projectile surface, thereby affecting both deformation and muzzle velocity. Sharper nose forms (e.g., B2, R = 6.135 mm) concentrated the gas pressure and reduced deformation, while broader nose geometries (e.g., B5, R = 6.951 mm) increased deformation but resulted in higher muzzle velocity. These findings demonstrate that nose geometry plays a decisive role in structural load distribution as well as aerodynamic acceleration.

Increasing propellant mass elevated the system’s energy level, as expected, but this increase did not fully translate into improved muzzle velocity. In the comparison of B1 (223 mg) and B7 (371.6 mg), although the propellant mass increased by 66%, the muzzle velocity rose by only about 8%. This indicates that a significant portion of the additional energy was dissipated as deformation and frictional losses. Therefore, an increase in energy input does not necessarily improve ballistic efficiency unless it is compatible with the rifling geometry.

Overall, the analyses demonstrate that barrel length, rifling density, nose geometry, and propellant mass are interdependent parameters. When evaluated collectively, the results reveal that an optimal balance must be established among linear velocity, rotational stability, and structural strength. Achieving such a balance enables both high muzzle velocity and extended barrel life.

Future studies may incorporate different firearm types, barrel lengths, rifling geometries, and projectile forms to expand the analysis. Such work would allow a broader investigation of the relationships among deformation, muzzle velocity, pressure distribution, and energy conversion efficiency across various system configurations.

These analyses can be performed not only in ANSYS but also using other finite element platforms such as Abaqus, LS-DYNA, or COMSOL Multiphysics. Comparative simulations across different software tools could improve accuracy and reliability.

Furthermore, incorporating thermal effects through thermo-mechanical coupling would enable the investigation of barrel life, thermal expansion, material softening, and fatigue behavior. The results may be validated through experimental studies, thereby increasing the scientific and industrial reliability of the design approach.

Acknowledgements

Funding/Financial Disclosure The authors have no received any financial support for the research, authorship, or publication of this study.

Ethics Committee Approval and Permissions The work does not require ethics committee approval and any private permission.

Conflict of Interests The authors stated that there is no conflict of interest in this article.

Authors Contribution The entire study including conceptual design, simulation modeling, data analysis, and manuscript preparation was conducted solely by the author [Ahmet Furkan ÖZBİLGE], who assumes full responsibility for the content of this work. All authors read and approved the final manuscript.

References

[1] D. E. Carlucci and S. S. Jacobson, *Ballistics: Theory and Design of Guns and Ammunition*, 2nd ed. Boca Raton, FL, USA: CRC Press, 2013.

[2] T. V. Nguyen and V. Q. Bui, “Studying the effect of rifling parameters on the stress state in a gun barrel wall when firing,” *Engineering and Technology Journal*, vol. 8, no. 8, pp. 2556–2564, 2023, doi: 10.47191/etj/v8i8.09.

[3] O. C. Zienkiewicz and R. L. Taylor, *The Finite Element Method*, 5th ed. Oxford, U.K.: Butterworth-Heinemann, 2000.

[4] Y. Yang *et al.*, "Dynamic stress analysis of anisotropic gun barrel under coupled thermo-mechanical loads via finite element method," *Latin American Journal of Solids and Structures*, vol. 17, no. 1, p. e243, 2020, doi: 10.1590/1679-78255800.

[5] M. Farhadi *et al.*, "Time-step sensitivity of ANSYS dynamic transient finite element modeling of fluid–structure interaction of bridge piers," *Computational Mechanics Journal*, 2019. [Online]. Available: https://www.researchgate.net/publication/333389073

[6] Ansys Inc., *ANSYS Mechanical User's Guide: Explicit Dynamics and Structural Analysis*. Canonsburg, PA, USA, 2023.

[7] H.-H. Lee, *Finite Element Simulations with ANSYS Workbench 2021*. Mission, KS, USA: SDC Publications, 2021.

[8] H. A. Wahl, *Mechanical Behavior of Materials*. Cambridge, U.K.: Cambridge University Press, 2016.

[9] R. K. Rajput, *Strength of Materials: Mechanics of Solids*. New Delhi, India: S. Chand Publishing, 2006.

[10] G. R. Liu and S. S. Quek, *The Finite Element Method: A Practical Course*. Oxford, U.K.: Butterworth-Heinemann, 2003.